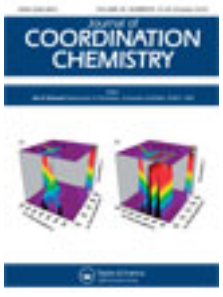

Journal of Coordination Chemistry
Publication details, including instructions for authors and subscription information:
http://www.tandfonline.com/loi/gcoo20

Dioxygen binding and activation by a highly reactive Cr(II) compound containing S,N-donors derived from o-aminothiophenol

Manjuri K. Koley [a], Seshadri C. Sivasubramanian [b], Sumit Biswas [c], Periakaruppan T. Manoharan [d] & Aditya P. Koley [e]

[a] Department of Chemical Engineering, Birla Institute of Technology and Science-Pilani, K.K. Birla Goa Campus, Zuarinagar 403726, Goa, India

[b] Department of Chemistry, Birla Institute of Technology and Science-Pilani, Pilani Campus, Pilani 333031, Rajasthan, India

[c] Department of Biological Sciences, Birla Institute of Technology and Science-Pilani, K.K. Birla Goa Campus, Goa 403726, India

[d] Department of Chemistry, Indian Institute of Technology-Madras, Chennai 600036, Tamil Nadu, India

[e] Department of Chemistry, Birla Institute of Technology and Science-Pilani, K.K. Birla Goa Campus, Zuarinagar 403726, Goa, India

Accepted author version posted online: 24 Jul 2012.Published online: 07 Aug 2012.

To cite this article: Manjuri K. Koley, Seshadri C. Sivasubramanian, Sumit Biswas, Periakaruppan T. Manoharan & Aditya P. Koley (2012) Dioxygen binding and activation by a highly reactive Cr(II) compound containing S,N-donors derived from o-aminothiophenol, Journal of Coordination Chemistry, 65:19, 3329-3351, DOI: 10.1080/00958972.2012.714867

To link to this article: http://dx.doi.org/10.1080/00958972.2012.714867

Journal of Coordination Chemistry
Vol. 65, No. 19, 10 October 2012, 3329–3351

Dioxygen binding and activation by a highly reactive Cr(II) compound containing S,N-donors derived from *o*-aminothiophenol

MANJURI K. KOLEY†, SESHADRI C. SIVASUBRAMANIAN‡, SUMIT BISWAS§, PERIAKARUPPAN T. MANOHARAN*¶ and ADITYA P. KOLEY*‖

†Department of Chemical Engineering, Birla Institute of Technology and Science-Pilani, K.K. Birla Goa Campus, Zuarinagar 403726, Goa, India
‡Department of Chemistry, Birla Institute of Technology and Science-Pilani, Pilani Campus, Pilani 333031, Rajasthan, India
§Department of Biological Sciences, Birla Institute of Technology and Science-Pilani, K.K. Birla Goa Campus, Goa 403726, India
¶Department of Chemistry, Indian Institute of Technology-Madras, Chennai 600036, Tamil Nadu, India
‖Department of Chemistry, Birla Institute of Technology and Science-Pilani, K.K. Birla Goa Campus, Zuarinagar 403726, Goa, India

(*Received 6 March 2012; in final form 26 June 2012*)

We report the synthesis, characterization, and reactivity of a Cr(II) complex, $[Cr(H_2O)(L^{ISQ})_2]$ (**1**) $[(L^{ISQ})^{1-}$ is *o*-iminothionebenzosemiquinonate(1−) π-radical], that is highly stable in solid state in the presence of air but undergoes spontaneous change in solution, both in the presence and absence of air. Physicochemical studies in solution show that a superoxo-Cr^{III} species, $[Cr(O_2)(OH)(L^{ISQ})_2]^-$ is generated initially in DMF solution of **1** in the presence of air owing to its immediate deprotonation followed by O_2 binding to the deprotonated species. The formation of this superoxo-Cr^{III} species is prominent and gradual in the presence of CH_3OH, a scavenger of CrO^{2+} species. This $Cr(O_2)^{2+}$ species in turn is converted to another highly reactive O=Cr(IV) intermediate $[O=Cr(OH)(L^{ISQ})_2]^-$ which undergoes disproportionation producing an unstable O=Cr(V) species, $[O=Cr(OH)(L^{ISQ})_2]$ and a stable Cr(III) compound, $[Cr(OH)(DMF)(L^{ISQ})_2]$ (**2**). The rate of this disproportionation is enhanced in the presence of $MnCl_2$, $[N(n\text{-}Bu)_4]PF_6$ and KSCN. The generated O=Cr(IV) species interacts with DNA with complete cleavage. The O=Cr(V) species slowly disappears from solution as revealed from EPR studies.

Keywords: Superoxo-Cr(III) complex; Oxo-chromium(IV) complex; Oxo-chromium(V) complex; EPR and electronic spectra; DNA interaction

1. Introduction

In order to get insight about the proposed high-valent Fe^{IV}=O intermediate responsible for the substrate oxidation step in catalytic cycles of oxygen-activating cytochrome

*Corresponding authors. Email: ptm@iitm.ac.in; koleyap@yahoo.co.in

ISSN 0095-8972 print/ISSN 1029-0389 online
http://dx.doi.org/10.1080/00958972.2012.714867

P450 and related mononuclear non-heme iron enzymes, there are several studies involving inorganic complexes in non-aqueous solvents that generate O=Fe(IV) species from their reactions with H_2O_2, ozone or peracetic acid carried out at low temperatures [1–4]. These studies have provided valuable information about this highly reactive O=Fe(IV) intermediate. Dioxygen activation has also been studied in inorganic systems containing Cr(II) centers. Scott *et al*. [5, 6] have shown using stopped-flow techniques that dioxygen spontaneously binds to Cr(II) in aqueous solution at room temperature leading to formation of either a superoxo-Cr(III), $[(H_2O)_5Cr(O_2)]^{2+}$ or an oxo-Cr(IV), $[(H_2O)_5CrO]^{2+}$ depending on the reaction conditions used and in the absence of any stabilizing ligands. The $[(H_2O)_5CrO]^{2+}$ species containing O=Cr(IV) is highly reactive and undergoes fast oxo transfer reaction with PPh_3 to produce $O{=}PPh_3$ quantitatively.

Theopold and co-workers [7a] have provided spectroscopic evidence showing that reaction of O_2 with a tris(pyrazolyl)borate chromium phenyl complex [$Tp^{tBu,Me}$Cr-Ph] ($Tp^{tBu,Me}$ = hydrotris(3-tert-butyl-5-methylpyrazolyl)borate) ultimately yielded a phenoxide, indicating insertion of oxygen into chromium-C bond through a superoxide-Cr^{III} intermediate and suggested a 'side-on' superoxide coordination to Cr^{III}. Starting from a four-coordinate Cr(II) precursor possessing the characteristic *cis*-divacant positions of an octahedral structure and by reacting it with excess O_2, Theopold and co-workers [7b] synthesized and isolated a stable six-coordinate superoxo-Cr^{III} compound, [$Tp^{tBu,Me}$Cr(Pz'H)(O_2)]BARF (pz'H = 3-tert-butyl-5-methylpyrazole, BARF = tetrakis(3,5-bis(trifluoromethyl)phenyl)borate), that was structurally characterized by X-ray crystallography which confirmed a ''side-on'' superoxide coordination to Cr^{III}. This low-spin superoxo-Cr(III) complex had effective magnetic moment of 2.8 BM resulting from antiferromagnetic coupling between the Cr(III) ion (d^3, $S = 3/2$) and the coordinated superoxide radical ($S = ½$). Very recently, Cho *et al*. have reported [8] an ''end-on'' chromium(III)-superoxo complex containing a macrocyclic TMC ligand (14-TMC = 1,4,8,11-tetramethyl-1,4,8,11-tetraazacyclotetradecane). The X-ray crystal structure of this compound showed the end-on superoxo-Cr(III) mononuclear complex in a distorted octahedral geometry [8a]. The reactivity of this complex has also been reported [8b].

There are several studies involving synthesis of stable O = Cr(IV) compounds in non-aqueous media. Autoxidation of Cr(II)porphyrin in toluene in the presence of air resulted in the formation of a highly stable diamagnetic O=Cr(IV)porphyrin complex that was isolated and structurally characterized by X-ray crystallography [9]. This oxo-Cr(IV) complex reacted [10] with triphenylphosphine to give triphenylphosphine oxide and chromium(II). The oxidation of β−phthalocyaninato chromium(II) compound by molecular oxygen or air, on the other hand, resulted in formation of a paramagnetic O=Cr(IV) complex [11]. The measured magnetic moment (1.9 BM at RT) for this complex was temperature dependent suggesting the presence of antiferromagnetic coupling between Cr ions.

Thus, interaction of O_2 with Cr(II) compounds either produces superoxo-Cr(III) or oxo-Cr(IV) species with different stabilities depending on the reaction conditions, solvents and the ligand environment around Cr(II). We have synthesized a Cr(II) compound, $[Cr(H_2O)(L^{ISQ})_2]$ (**1**), containing [12–14] two *o*-iminothionebenzosemiquinonate(1−) π-radicals $(L^{ISQ})^{1-}$ and one water as the coordinated ligands which is very different from the reported blue Cr(II) bischelate complex $[Cr(L^{AP})_2]$ (where $(L^{AP})^{1-}$ is the *o*-aminothiophenolate(1−)) that was synthesized by Larkworthy *et al*. [15] in dinitrogen atmosphere. Compound **1** is

highly stable at RT in the presence of air but when dissolved in DMF, undergoes spontaneous change in solution at RT, both in the absence and presence of air, clearly indicating highly reactive compound. This strongly suggests that the chemistry of chromium compound containing this ligand is complex and a challenging problem to study. This could be the major reason for not having any other report of chromium compounds with this ligand *o*-aminothiophenol after that reported by Larkworthy *et al.* [15] over 40 years ago. Here, we describe the synthesis, characterization, and spectroscopic changes as well as reactivity in solution for **1**.

2. Experimental

2.1. *General remarks*

Cr compounds are carcinogenic. Necessary precautions must be taken to avoid skin contact and inhalation of their solutions and dusts.

2.2. *Materials*

o-Aminothiophenol, triphenylphosphine, triphenylphosphine oxide and $[N(n\text{-}Bu)_4]PF_6$ (tetrabutylammonium hexafluorophosphate) were obtained from Aldrich. $Cr(NO_3)_3 \cdot 9H_2O$ was obtained from Merck. Absolute ethanol (GR), methanol (GR), dichloromethane (GR), toluene (GR), N,N-dimethyl formamide (DMF) (GR) and acetonitrile (HPLC) were also obtained from Merck. All other chemicals were of reagent grade and used as such.

2.3. *Preparation of* $[Cr(H_2O)(L^{ISQ})_2]$ *(1)*

A solution of $Cr(NO_3)_3 \cdot 9H_2O$ (0.4 g, 1 mmol) dissolved in 15 mL of absolute ethanol was slowly added to a solution of *o*-aminothiophenol (0.250 g, 2 mmol) in 50 mL of dehydrated ethanol with constant stirring at room temperature. Stirring was continued for 2 h in the presence of air while the solution turned yellow–brown and a dark compound separated from the solution. This was filtered, and the residue was washed with ethanol and air dried. Then the compound was thoroughly washed with water until free from any acid and dried. Finally the compound was washed again with ethanol and dried in vacuum. The color of **1** was almost black. Yield: 50%. Anal. Calcd for $C_{12}H_{12}N_2S_2OCr$ (%): C, 45.55; H, 3.83; N, 8.86. Found (%): C, 45.67; H, 3.90; N, 8.95.

The mother filtrate obtained after filtering the dark compound mentioned above was collected and dried in vacuum. Then the residue was stirred with CH_2Cl_2/ether (1 : 1) and filtered. Evaporation of this solution followed by recrystallization from toluene yielded a yellow compound which turned out to be 2,2′-dithiodianiline as identified from its melting point (93°C), and by comparing its IR and electronic spectra with that of an authentic sample of 2,2′-dithiodianiline.

2.4. *Decomposition product [Cr(OH)(L^{ISQ})$_2$(DMF)] (2) from DMF*

Compound **1** (50 mg, 0.158 mmol) was dissolved in 50 mL of DMF in a stoppered conical flask and stirred at room temperature for 72 h in presence of air. This solution was then filtered through a sintered glass crucible and the solvent was evaporated *in vacuo* to a small volume when a dark compound separated. This was filtered and the dark residue was redissolved in a minimum of DMF, and CH_2Cl_2 and hexanes were then added to precipitate a black solid which was collected by filtration and washed with CH_2Cl_2 and dried under vacuum. Yield: 25 mg. Anal. Calcd for $C_{15}H_{18}N_3S_2O_2Cr$ (%): C, 46.37; H, 4.67; N, 10.82. Found (%): C, 46.51; H, 4.72; N, 11.02.

2.5. *Interaction with DNA*

To check the effect of different species that were generated with time in DMF solution of **1** in presence of air on double stranded DNA, 1 μL solution was drawn at specific times from a DMF stock solution of **1** (63.3×10^3 μM L^{-1}) and each time this was added immediately to 2 μL solution of DNA (0.6×10^{-6} μM L^{-1}) in TAE buffer (Tris Acetate EDTA, pH 8.0) and this mixture was incubated for 30 s before adding DNA loading dye and placed in the well of the agarose gel (1.2%). Initial experiments showed that samples taken during the first 12 min from the time of making the DMF solution of **1** have no effect on DNA. However, samples taken from the DMF stock solution in the 13th, 14th, and 15th min from the time of making the solution were found to have drastic effect on DNA. After this time span, the solution again has no effect on DNA. To demonstrate this, sample (1 μL DMF solution of **1** with time for each sample) was taken in the 5th min from the time of making the solution and this was added immediately to 2 μL solution of DNA substrates; this mixture was incubated for 30 s and then added with the DNA loading dye and placed in the well of the agarose gel. Then samples were taken every 1 min interval starting from the 11th min up to the 19th min from the time of making the DMF solution and each of these samples was added immediately to 2 μL solution of DNA substrates that were already aliquoted out separately in different tubes, and then each of these mixtures (sample + DNA) was incubated for 30 s before adding with the DNA loading dye and placed in the individual wells of the agarose gel. The effect of different species that were generated with time in DMF solution of **1** on the DNA was then checked by running these different mixtures placed in different wells of the agarose gel. A positive control wherein the same concentration of the DNA was treated with DNAseI at RT for 30 min and a negative control (DNA in TAE) were also simultaneously run in the gel. This experiment was repeated three times and the reproducibility of the results was verified. Identical results were obtained when the experiments were performed using the DNA solution in TAE buffer at pH 7.4 and keeping all other parameters the same.

2.6. *Physical measurements*

Elemental analyses (for C, H, and N) were performed on a Perkin-Elmer model 2400 series II CHNS analyzer. Infrared spectra were measured with Jasco IR report-100 and a Shimadzu 8400S FT-IR spectrometers using KBr pellets. Static susceptibility measurement was made with the help of a Lakeshore VSM 7410 Vibrating Sample

Magnetometer. Electronic spectra were recorded with a Jasco V-570 UV/VIS/NIR spectrophotometer using a pair of matched quartz cells of path length of 1 cm. EPR spectra were recorded using a Bruker spectrometer operating at X-band and a Varian E-112 X/Q-band spectrometer. Instrumental parameters: modulation frequency = 100 kHz, modulation amplitude = 1 G, microwave power = 20 mW. RT solution EPR spectra were recorded using an aqueous cell. Frozen glass and liquid nitrogen temperature (LNT) EPR spectra were recorded in liquid nitrogen using a quartz dewar. Diphenylpicrylhydrazyl (DPPH) was used as internal field marker. X-ray photoelectron spectra (XPS) were recorded on a VG Microtech Multilab ESCA 3000 spectrometer. All measurements were made [16, 17] at room temperature (298 K) using a nonmonochromated Mg-Kα X-ray source ($h\nu = 1253.6$ eV) on powder samples and pressure in the analysis chamber was maintained at $3 - 6 \times 10^{-10}$ Torr. The energy resolution of the spectrometer was measured from the full width at half-maximum of metallic gold, and the value obtained was better than 0.8 eV with Mg-Kα radiation at a pass energy of 20 eV. Binding energy (BE) calibration was performed with Au $4f_{7/2}$ core level (83.9 eV). BE of adventitious carbon (284.9 eV) was utilized for charge correction for all core-level spectra. The error in the reported BE values is ± 0.1 eV. Conductivity and pH measurements were done using a Mettler Toledo dual conductivity/pH meter model SevenMulti equipped with Inlab 730 and Inlab 413 electrodes. Electrochemical measurements were done with the help of a Bioanalytical system CV-27 electrochemical analyzer and a BAS model X-Y recorder at 298 K under dinitrogen. A standard three-electrode cell consisting of a platinum working electrode, a platinum auxiliary electrode and a Ag/AgCl reference electrode was used. Tetraethylammonium perchlorate (TEAP) was used as supporting electrolyte.

3. Results and discussion

The reaction of $Cr(NO_3)_3 \cdot 9H_2O$ and *o*-aminothiophenol in absolute ethanol at RT in the presence of air resulted in isolation of **1**. Since the synthesis was carried out in dehydrated ethanol, the source of the coordinated water in **1** is most likely $Cr(NO_3)_3 \cdot 9H_2O$. Compound **1** is insoluble in common organic solvents like CH_3OH, C_2H_5OH, and toluene, and poorly soluble in CH_2Cl_2, CH_3CN, and acetone producing a light pink solution, but this color is discharged with time. The compound is readily soluble in DMF producing initially a light brown solution that changes to intense purple within a few minutes; it continues to change to wine red and ultimately to a light pink solution. Thus, this compound is not stable in any of these solvents and undergoes spontaneous change in solution even in the absence of air as revealed from the electronic spectral studies in a nitrogen atmosphere (*vide infra*) preventing its recrystallization. Though it was not possible to recrystallize the compound, this compound was synthesized several times and the consistency in repeated elemental analyses showed its purity and reproducibility. It appears that **1**, like many other Cr(II) compounds, undergoes rapid oxidation in solution in the presence of air to generate initially a superoxo-Cr^{III} compound and then another O=Cr(IV) intermediate which undergoes disproportionation [18, 19] to produce a O=Cr(V) and a Cr(III) species. This O=Cr(V) species was also unstable in solution and eventually leads to a low absorbing Cr(III) compound as evident from the following results.

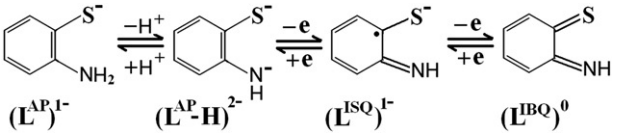

Scheme 1. Four forms of *o*-aminothiophenol that differ in their protonation and oxidation states.

3.1. *Infrared spectra*

IR spectra of the compounds were recorded using KBr pellets. The spectrum of **1** exhibits a broad band centered at 3433 cm^{-1} (figure S1), indicating the presence of coordinated water [20] in the compound. A medium intensity sharp band at 3240 cm^{-1} along with a shoulder near 3275 cm^{-1} likely arises from ν(N–H) [21]. The $\delta(NH_2)$ and the aromatic C–NH_2 stretching bands which appear as two strong bands at 1610 and 1300 cm^{-1}, respectively, in the free HL^{AP} spectrum are absent in the IR spectrum of **1**, indicating deprotonation of the $-NH_2$ groups in the complex. An intense band at 1116 cm^{-1} (figure S1) indicates the presence of $\nu(CS^{\bullet})$. This band has already been established as a marker [22–28] for the presence of the π-radical anion for a number of dithiolene and analogous coordination compounds. This indicates that the ligand is coordinated in the form of $(L^{ISQ})^{1-}$ in **1**. The possibility of the band around 3433 cm^{-1} originating from absorbed H_2O in KBr is ruled out since strong O 1s peak is observed from the XPS studies of "KBr-free" pure powder sample of **1** (*vide infra*).

Compound **2**, on the other hand, exhibits bands around 3450 and 3350 cm^{-1}, possibly due to ν(OH) and ν(NH), respectively, and the presence of DMF is indicated from the appearance of ν(CO) at 1642 cm^{-1}, while the π(C–H) for the *o*-disubstituted benzene ring appears at 745 cm^{-1}. The strong band at 1116 cm^{-1} due to $\nu(CS^{\bullet})$ observed for **1** is also observed for **2** but its intensity is less.

Four forms of *o*-aminothiophenol (L) and substituted *o*-aminothiophenol (L_1) that differ in their protonation and oxidation states have been established unequivocally by Wieghardt and coworkers [12–14], as shown in scheme 1.

They have shown that apart from the monoanion *o*-aminothiophenolate(1–) $(L^{AP})^{1-}$ and the dianion *o*-imidothiophenolato(2–) $(L^{AP}-H)^{2-}$, the *o*-iminothionebenzosemiquinonate(1–) π-radical $(L^{ISQ})^{1-}$ is present in many transition metal complexes [14, 22, 23] that are synthesized in air. Thus reaction of $Cr(NO_3)_3 \cdot 9H_2O$ with *o*-aminothiophenol in absolute ethanol at RT in air leading to formation of **1** can be represented as shown in scheme 2.

In our present experimental conditions, it is highly unlikely that the ligand is coordinated either in the form of monoanion $(L^{AP})^{1-}$ or neutral $(L^{IBQ})^{0}$. Considering the oxidation state of the starting material (Cr^{III}), it is possible that the oxidation state of the metal ion in **1** is either +3 or +2. In the case of +3 oxidation state, out of the two chelating ligands evident from the elemental analysis, one should be present as the dianion *o*-imidothiophenolato(2–) $(L^{AP}-H)^{2-}$ and the other as *o*-iminothionebenzosemiquinonate(1–) π-radical $(L^{ISQ})^{1-}$, since no other anion is present in this complex. For +2 oxidation state of the metal ion, both the ligands should be present as *o*-iminothionebenzosemiquinonate(1–) π-radical $(L^{ISQ})^{1-}$. The electronic spectrum of **1** in DMF (*vide infra*) did not display any intense absorption in the near-infrared region (>600 nm), which was expected to appear as an intervalence charge-transfer (IVCT) band [22, 23] between a $(L^{AP}-H)^{2-}$ and $(L^{ISQ})^{1-}$, considered to be a

$$Cr(NO_3)_3{\cdot}9H_2O \xrightarrow[EtOH,\ O_2]{L^{AP}} [Cr(H_2O)(L^{ISQ})_2]\ (1)$$

Scheme 2. Synthesis of **1** from reaction of Cr(III) with *o*-aminothiophenol in ethanol in the presence of air.

marker for the presence of ligand mixed valency as for Cr(III) coordinated to two chelating ligands in these two different oxidation states. Thus, it is likely that both ligands are present as *o*-iminothionebenzosemiquinonate(1−) π-radical $(L^{ISQ})^{1-}$ forming a Cr(II) complex. In the presence of the thiol Cr(III) is reduced to Cr(II) which then coordinates to the remaining thiol ligand as indicated from its low yield as well as from formation of the oxidized ligand dimer, 2,2′-dithiodianiline. Reduction of metal ion followed by coordination of the thiol ligand in its oxidized form is reported by Kapre *et al.* [23] for synthesis of Mo(V) compounds starting from $[MoO_2(acac)_2]$ in the presence of air. It is not unlikely that Cr(II) is coordinated to the oxidized *o*-iminothionebenzosemiquinonate(1−) π-radical $(L^{ISQ})^{1-}$ in the present case and also, as mentioned earlier, this compound is very different from the reported blue Cr(II) bischelate complex $[Cr(L^{AP})_2]$ that was synthesized in dinitrogen atmosphere with *o*-aminothiophenol by Larkworthy *et al.* [15]. The magnetic moment of this compound was reported to be 4.71 BM at 322.5 K and the ν_{max} was observed in the visible spectrum at 16 900 cm^{-1} [15].

3.2. *X-ray photoelectron spectra*

The peak positions of Cr $2p_{3/2}$ and $2p_{1/2}$, S 2p, C 1s, N 1s, and O 1s signals for both **1** and **2** are presented in table 1. The binding energy shifts (ΔE's) were calculated by taking the E° values [29–32] for Cr $2p_{3/2}$, S 2p, O 1s, N ls, and C 1s as 574.1, 164.8, 531.6, 401.6, and 284.9 eV, respectively, and are also presented in table 1. In the observed ESCA spectra Cr $2p_{3/2}$ and $2p_{1/2}$ signals appear at 576.7 and 586.0 eV for **1**, while Cr $2p_{3/2}$ and $2p_{1/2}$ signals for **2** appear at 577.6 and 587.0 eV, respectively.

Thus, the Cr $2p_{3/2}$ binding energy for **1** is almost 1 eV lower than that observed for **2**, strongly suggesting the difference in their metal ion oxidation states because their ligand environments are similar. It may be mentioned here that the Cr $2p_{3/2}$ binding energy for **2** is similar to those reported for Cr(III) compounds like $CrCl_3$, $Cr(OH)_3$, $Cr(NO_3)_3$ and $Cr(acac)_3$ (acac = acetylacetonate anion) [29–32], while the Cr $2p_{3/2}$ and $2p_{1/2}$ binding energies for **1** are very similar to the reported values (576.9 and 585.9 eV for Cr $2p_{3/2}$ and $2p_{1/2}$, respectively) for $Cr(\pi C_5H_5)_2$ with +2 oxidation state for this metal ion [33]. But, a direct comparison with the reported values is not possible in the absence of data with similar ligands. However, the Cr $2p_{3/2}$ binding energy difference of ~1 eV between **1** and **2** is significant and consistent with the formulation of Cr(II) and Cr(III) oxidation states for **1** and **2**, respectively. The strong O 1s peak at 531.5 eV (figure S2) for **1** and that at 531.8 eV for **2** confirm its presence in these two compounds.

3.3. *Magnetic moments*

The room temperature (at 27°C) magnetic susceptibility measurement for **1** shows $\mu_{eff} = 2.76$ BM while that for **2** is 1.8 BM. This suggests that the two ligand π-radical

Table 1. Core electron binding energies (BE) and ΔE (eV) for **1** and **2**.

	Compound **1**		Compound **2**	
Peaks	BE	ΔE	BE	ΔE
Cr $2p_{3/2}$	576.7	2.6	577.6	3.5
Cr $2p_{1/2}$	586.0		587.0	
S 2p	162.8	−2.0	164.0	−0.8
N 1s	400.2	−1.4	399.8	−1.8
C 1s	286.2	1.3	285.0	0.1
O 1s	531.5	−0.1	531.8	0.2

anions in **1** have resulted $S_t = 1$ from strong antiferromagnetic coupling between the Cr(II) ($3d^4$) and the coordinated ligand π-radical anions ($S = ½$) with an effective magnetic moment of around 2.8 BM. On the other hand, the d^3 Cr(III) ion and the two ligand π-radical anions in **2** have resulted $S_t = ½$ ground state from their strong antiferromagnetic coupling of the same kind. It is to be noted here that for the reported $[M^{II}(L^{ISQ})_2]$, where M = Ni, Pd, and Pt, $S_t = 0$, while for $[Fe^{III}(L_1^{ISQ})_2X]$ where X = Cl, Br, or I, $S_t = ½$, suggesting strong antiferromagnetic coupling in all these cases [12–14]. Such strong antiferromagnetic coupling is also observed for the Cr(III) compounds reported by Kapre *et al.* [22] who isolated the neutral complex $[Cr^{III}(^{3,6}L^{\bullet}_{sq})_3]$ which has $S = 0$. This compound on reduction with $[Co(Cp)_2]$ in CH_2Cl_2 gave $[Co(Cp)_2][Cr^{III}(^{3,6}L^{\bullet}_{sq})_2(^{3,6}L_{cat})]$ with $S = ½$, where $H_2[^{3,6}L_{cat}]$ is the 3,6-di-tert-butylcatechol, $(^{3,6}L^{\bullet}_{sq})^{1-}$ is the π-radical monoanionic *o*-semiquinonate of the catecholate dianion $(^{3,6}L_{cat})^{2-}$, and $Co(Cp)_2$ is cobaltocene. They have also reported the isolation of the corresponding $[N(n\text{-}Bu)_4][Cr^{III}(^{3,5}L^{\bullet}_{ss})_2(^{3,5}L_{ss})]$, where $(^{3,5}L_{ss})^{2-}$ represents the dianion 3,5-di-tert-butylbenzene-1,2-dithiolate(2−) and $(^{3,5}L^{\bullet}_{ss})^{1-}$ is its π-radical monoanion. This latter complex also has $S = ½$. In the present cases, the observed magnetic moment values along with strong and broad RT EPR signals exhibited by **1** and **2** at X-band (*vide infra*) clearly rules out $S_t = 0$.

Thus, we propose a strongly antiferromagnetically coupled Cr(II) complex containing two π-radical *o*-iminothionebenzosemiquinonate(1−) (L^{ISQ}) ligands and a coordinated water resulting in $S_t = 1$ for **1**. Hence, **1** should have one of the two structures shown in scheme 3.

3.4. *EPR studies*

The powder EPR spectrum for **1** is recorded at X-band frequency at RT. The compound exhibits a strong and broad spectrum [figure 1 (panel A)] with a peak-to-peak line width of 500 G with $g = 1.972$ in the powder state indicating that it is paramagnetic. This line becomes even broader (figure not shown) when the powder spectrum is recorded at LNT, as evident from the peak-to-peak line width of ~800 G with $g = 2.039$. Low temperature broadening and change in *g*-value is a reflection of antiferromagnetic coupling between Cr(II) and the ligand radicals.

When **1** is dissolved in DMF in the presence of air and RT solution spectrum is recorded, it exhibits a EPR signal consisting of a strong central line (at $g = 1.99$) with indication of hyperfine features and flanked by two weak satellites [figure 1 (panels B

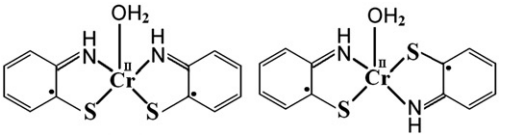

Scheme 3. Proposed structures for **1**.

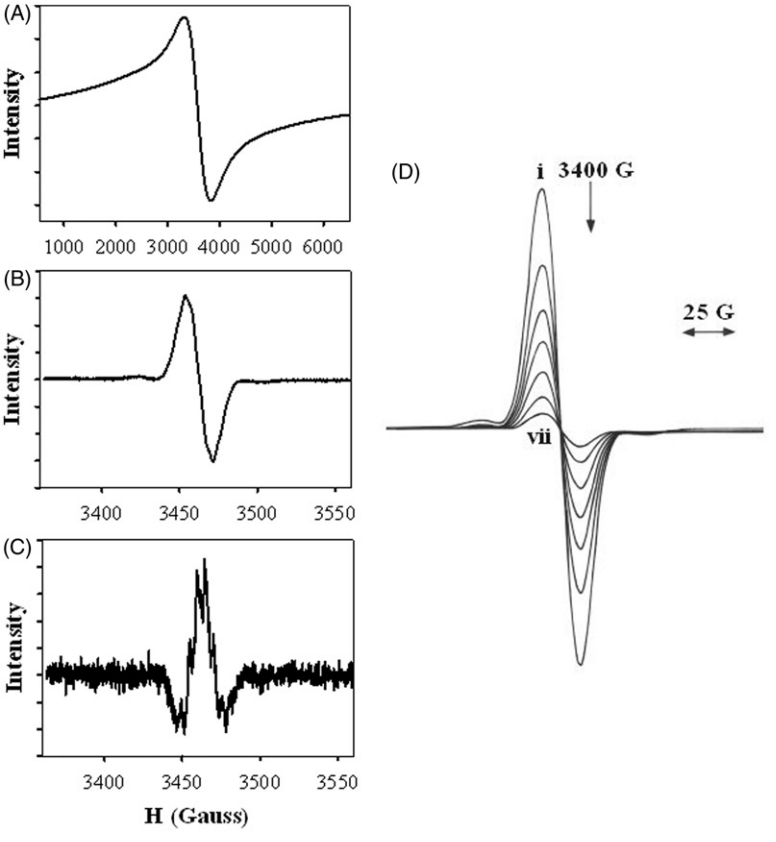

Figure 1. X-band EPR spectra of $[Cr(H_2O)(L^{ISQ})_2]$ (**1**). Panel A: Powder sample at RT without DPPH. Panel B: First derivative spectrum of DMF solution (2.5×10^{-3} mol L^{-1}) at RT recorded in the presence of air. Panel C: Second derivative spectrum. Panel D: EPR spectral change of **1** (3×10^{-3} mol L^{-1}) in DMF solution in presence of air at RT showing the disappearance of the Cr(V) signal with time (after reaching maximum intensity). Time taken for this decay shown in traces (i)–(vii) is 90 min.

and C)] possibly originating from a d^1 Cr(V) species. However, the intensity of this signal initially increases with time (figure S3) indicating increase in concentration of the Cr(V) species responsible for this signal and then after reaching a maximum intensity, it starts decreasing slowly [figure 1 (panel D)] possibly due to the decomposition in solution. The EPR spectrum of a d^1 Cr(V) species should consist of a single isotropic line ($I = 0$ for ^{52}Cr, 90.45% abundance) accompanied by a four-component hyperfine structure due to ^{53}Cr isotope ($I = 3/2$, with a natural abundance of 9.55%). However, in

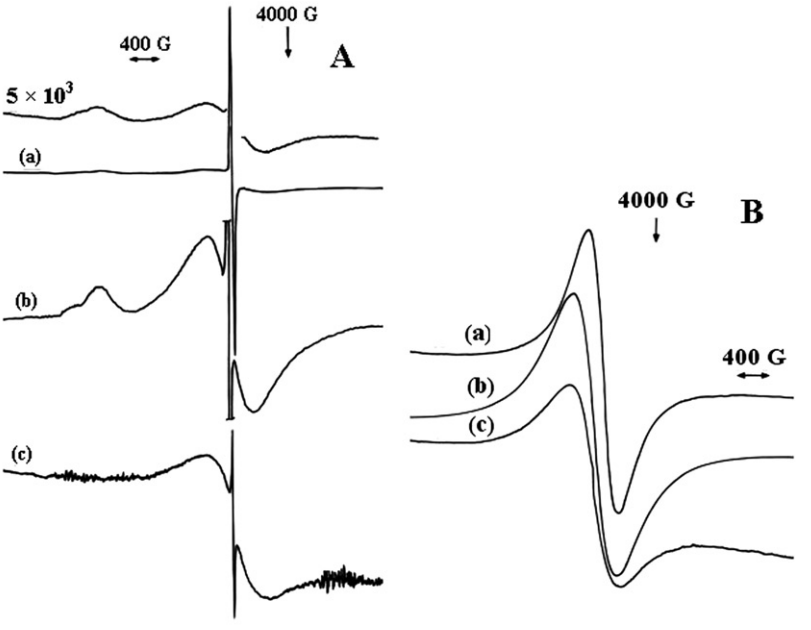

Figure 2. Panel A: Frozen glass EPR spectra recorded (without DPPH) at X-band frequency at LNT for **1** (3×10^{-3} mol L^{-1}) in DMF in the presence of air showing the changes in the spectrum as time progresses. (a) Frozen glass spectrum recorded within 5 min after making a fresh DMF solution. (b) After recording spectrum shown in (a), the solution was brought back to RT and frozen again (recorded within 15 min of making the fresh DMF solution). (c) Frozen glass spectrum recorded after keeping the above solution at RT for ~5 h. Panel B: X-band EPR spectra of **2** without DPPH. (a) RT powder. (b) LNT powder. (c) DMF frozen glass at LNT.

the present case, the weak satellite lines appearing along with central line seem to be the extreme end hyperfine lines of ^{53}Cr as indicated not only by A values calculated (20 G) and reported [34] for similar species but also from their relative intensity ratio with respect to the central line due to ^{52}Cr. The hyperfine structure of the central line is clearly evident from the second derivative spectrum [figure 1 (panel C)], indicating hyperfine interaction with a number of ^{14}N and ^{1}H nuclei.

The frozen glass LNT spectrum of a freshly prepared DMF solution of **1** in the presence of air is shown in figure 2 ((a) in panel A). When this solution is brought to room temperature and then frozen again within a couple of minutes, the frozen glass EPR spectrum [figure 2 ((b) in panel A)] is different than the initial one. Then this solution is kept at room temperature for several hours and then again its frozen glass EPR spectrum is recorded. This spectrum [figure 2 ((c) in panel A)] exhibits a single broad line along with a sharp central line instead of two broad lines along with the strong central line initially observed in the frozen glass spectrum indicating the presence of a Cr(III) species (broad line) and possibly an O=Cr(V) species (sharp central line) in the resultant solution. This sharp central line ultimately disappeared and only the broad spectrum remained when the solution was kept at RT for two days and then its frozen glass spectrum was recorded (figure not shown). This is consistent with the slow disappearance of the RT DMF solution EPR signal shown in figure 1 (panel D), strongly suggesting that the Cr(V) species slowly disappears from the solution.

Compound **2**, on the other hand, exhibited broad spectrum in the powder state [figure 2 (panel B)] indicating that it is also paramagnetic. The powder EPR spectrum [figure 2 ((a) in panel B)] showed a peak-to-peak line width of 400 G with $g = 1.98$ at RT. This line became even broader when the powder spectrum was recorded at LNT [figure 2 ((b) in panel B)] as evident from the peak-to-peak line width of 600 G with $g = 2.04$. The DMF frozen glass spectrum was also broad [figure 2 ((c) in panel B)]. Thus, the powder samples of **1** and **2** show similar EPR behavior, both at RT and LNT, except for a little reduced line width in **2**, suggesting the presence of antiferromagnetic coupling between the Cr(III) and the free radical ligands in this latter compound also. The reduced line width in **2** as compared to **1** is possibly due to the stronger Cr(III)–hydroxide in **2** than the Cr(II)–H_2O bonding in **1**. In addition, the presence of DMF in **2** must have caused a reduction in dipolar broadening due to increased intermolecular separations.

3.5. *Conductivity and pH measurements*

Another interesting observation is the change of conductivity and pH of the DMF solution of **1**. First conductivity and pH were measured for DMF (50 mL) solvent only, then 7.0 mg (0.022 mmol) of **1** was added and stirred for a minute with a magnetic stirrer to dissolve the compound (conc. 4.43×10^{-4} M) at RT and conductivity and pH were measured. There is an immediate increase in conductivity (from 9.48 $\mu S\,cm^{-1}$ of DMF only to 11.58 $\mu S\,cm^{-1}$) and decrease in the pH of the DMF solution, and this trend continues rapidly up to 20 min and then continues to change slowly (figure S4). Though the pH change in non-aqueous solvent is difficult to quantify, the measurement of conductivity in solution is reliable for ionic species present or produced in aqueous as well as in non-aqueous solutions. Thus the decrease in pH (taking the pH of the pure DMF as the reference) followed by increase in conductivity (from 9.48 $\mu S\,cm^{-1}$ of DMF to finally 17.50 $\mu S\,cm^{-1}$ in presence of **1**) with time clearly indicates the formation of ionic species due to deprotonation of the aqua ligand (the organic ligands are already deprotonated). This deprotonation occurs spontaneously either in the absence or presence of air and it is most likely associated with the formation of a $Cr^{II}(OH)^-$ species which has a strong absorbance at 474 nm and readily binds to dioxygen (*vide infra*). The conductivity studies, however, do not show enough change to be an electrolyte, but appears to be more consistent with an equilibrium from a weak electrolyte as shown in equation (1).

$$\left[Cr(H_2O)(L^{ISQ})_2\right] \rightleftharpoons \left[Cr(OH)(L^{ISQ})_2\right]^- + H^+ \quad (1)$$

3.6. *Electronic spectra*

3.6.1. DMF solution. Figure 3 (panel A) shows the electronic spectrum of **1** in DMF that was recorded immediately (within 1 min) after making a fresh solution in the presence of air. The spectrum initially shows a strong band at 474 nm with a weak shoulder at ~543 nm followed by strong absorptions in the UV region and the absorbance in the NIR and lower energy of the visible region (up to 600 nm) is found to be very low [figure 3 (panel A, curve (a))]. However, the second scan (within 5 min) shows a strong band appearing at 543 nm along with another strong band at 457 nm

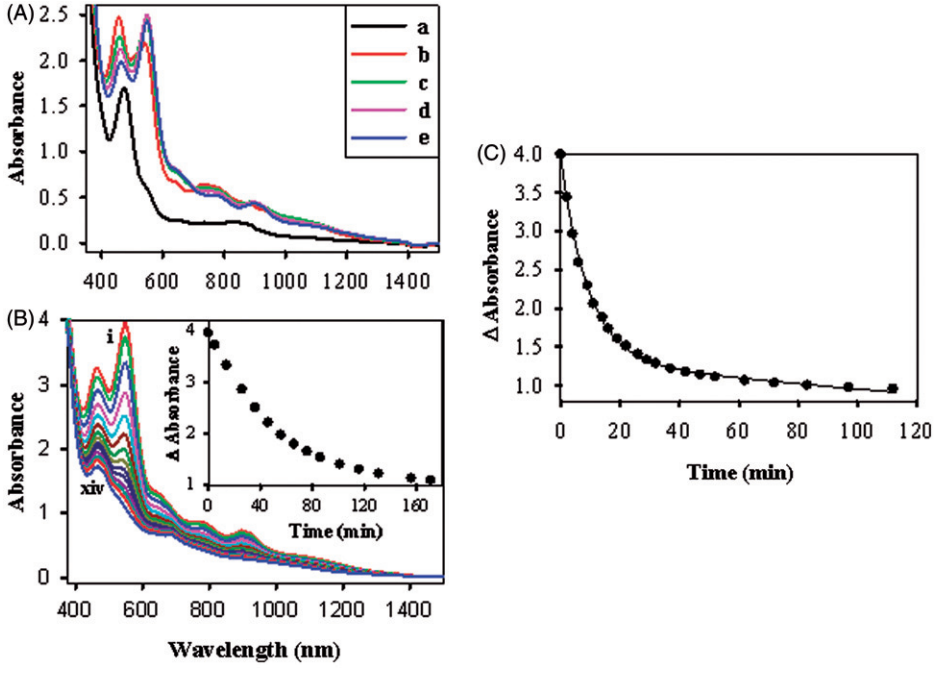

Figure 3. Panel A: Electronic spectral changes of $[Cr(H_2O)(L^{ISQ})_2]$ (**1**) (7.23×10^{-4} mol L^{-1}) in DMF in the presence of air. (a) Within 2 min (black) and (d) when reaching maximum intensity at 548 nm in 14 min (purple). Panel B. Electronic spectral change of $[Cr(H_2O)(L^{ISQ})_2]$ (**1**) (1.16×10^{-3} mol L^{-1}) in DMF in the presence of air for disappearance of 548 nm band in the absence of PPh_3: (i) at 14th min when absorbance reached maximum intensity at 548 nm, (xiv) when 548 nm peak almost disappeared. Inset: Plot of absorbance change at 548 nm *vs.* time. Panel C: Plot of absorbance change for the disappearance of the band at 548 nm *vs.* time of $[Cr(H_2O)(L^{ISQ})_2]$ (**1**) (1.16×10^{-3} mol L^{-1}) in DMF in presence of two-fold excess of Mn^{2+} (in the presence of air) along with a two exponential fit (—) using the model $\Delta A_t = a_1 e^{-k_1 t} + a_2 e^{-k_2 t}$.

and a few weak bands in the lower energy of the visible and in the NIR regions [figure 3 (panel A, red curve (b))]. Ultimately, two very strong bands resulted at 464 and 548 nm in the visible region along with four weaker bands at 640, 763, 896, and 1050 nm, and these bands reached maximum intensity within 14 min [figure 3 (panel A, purple curve (d))]. Intensities of all these bands started decreasing slowly with time [figure 3 (panel A, blue curve (e))]. At this point when the 548 nm band reached maximum intensity, a highly reactive intermediate is generated which interacts with DNA leading to its complete cleavage (*vide infra*).

When the 548 nm peak reached maximum intensity, solid PPh_3 was added and spectra were recorded to monitor the disappearance of this band with time. This is shown in figure S5.

The disappearance of the 548 nm peak after it reached maximum intensity is also studied in the absence of PPh_3 and is shown in figure 3, panel B. The intensities of all the bands in the visible and NIR regions start slowly decreasing with time and this spectral change does not involve any isosbestic point. The change in absorbance at 548 nm with time is shown in the inset of figure 3 (panel B).

Addition of PPh_3 to the resultant solution, as shown in figure 3 (panel B), showed further change in the spectrum indicating a prompt reaction. This change is shown in figure S6(xiv–xxi). Evaporation of this solution or that mentioned in figure S5, after

completion of the reaction with PPh_3 followed by purification yielded a mixture of some chromium compounds and free O=PPh_3 in both cases. This latter compound was recrystallized from CH_2Cl_2–toluene and characterized by comparing its IR and electronic spectra and its melting point with that of an authentic sample of triphenylphosphine oxide. Thus formation of O=PPh_3 from the reaction with PPh_3 in both cases strongly suggests the presence of a Cr(IV) and/or a Cr(V) species that is capable of *oxo* transfer reactions [5]. If the resultant solution shown in figure 3(xiv) in panel B is allowed to stand for two days at RT without adding PPh_3, it also leads to a low absorbing species as revealed from its electronic spectrum (figure not shown) possibly due to the decomposition of the Cr(V) species generated in solution and ultimately producing a Cr(III) species. This is consistent with the disappearance of the RT EPR signal of the DMF solution [figure 1 (panel D)] as well as the central sharp line from the frozen glass EPR spectrum obtained after keeping the DMF solution of **1** at RT for 2 days (discussed earlier). The properties of isolated **2** are also consistent with Cr(III) formulation.

The decay of the 548 nm peak of **1** in DMF at RT with time was also studied in the presence of two-fold excess of Mn^{2+} which is known as a Cr(IV)–specific reductant [18, 19, 35, 36] and found that the decay of this peak in the presence of Mn^{2+} is much faster [figure 3 (panel C)] than that in the absence of Mn^{2+} ion [figure 3 (panel B inset)]. This strongly suggests that the absorbance at 548 nm originates from a reactive O=Cr(IV) species which undergoes disproportionation that can be accelerated by Mn^{2+}.

These data [figure 3 (panel C)] were fitted using the two exponential model $\Delta A_t = a_1 e^{-k_1 t} + a_2 e^{-k_2 t}$, which yielded $a_1 = 2.60 \pm 0.04$, $k_1 = 0.111 \pm 0.003$, $a_2 = 1.35 \pm 0.03$, and $k_2 = 0.0034 \pm 0.0004\,\text{min}^{-1}$, respectively. This clearly shows the involvement of two species that are associated with the decay of the 548 nm peak in the presence of Mn^{2+} and is consistent with the proposed mechanism (discussed later).

The fact that the DMF solution contains a highly reactive intermediate O=Cr(IV) species is also evident from the following observation. Upon addition of millimolar quantities of CH_3OH to the purple DMF solution when the 548 nm peak reached maximum intensity [figure S7 (panel A)], it started disappearing much faster than the uncatalyzed decay shown in figure 3, and the disappearance of the 548 nm peak was complete within 70 min [figure S7 (panel B)] as compared to >200 min in the absence of CH_3OH [figure 3 (panel B)]. CH_3OH undergoes two-electron oxidation by highly reactive O=Cr(IV) intermediates as reported by Scott *et al.* [5, 6] and it has been used as a scavenger of CrO^{2+}. Thus, we suggest that the species associated with the 548 nm peak in DMF solution is a short lived O=Cr(IV) intermediate generated from air oxidation of **1** in DMF solution.

3.6.2. DMF + CH_3OH solution. Very interesting electronic spectral results were obtained when **1** was dissolved in DMF that already contained excess CH_3OH (2 : 1). Figure 4 (panel A) shows the electronic spectrum of **1** in DMF + CH_3OH (2 : 1) that was recorded immediately (within one min) after making a fresh solution in the presence of air. The spectrum initially shows only a strong band at 474 nm with a very weak and broad band centred at ~549 nm followed by strong absorptions in the UV region, but the absorbance in the NIR and lower energy of the visible region (up to 600 nm) is found to be very low [figure 4 (panel A, black curve)]. However, the second scan shows an increase in intensity for the 474 nm band with overall increase in absorbance for all

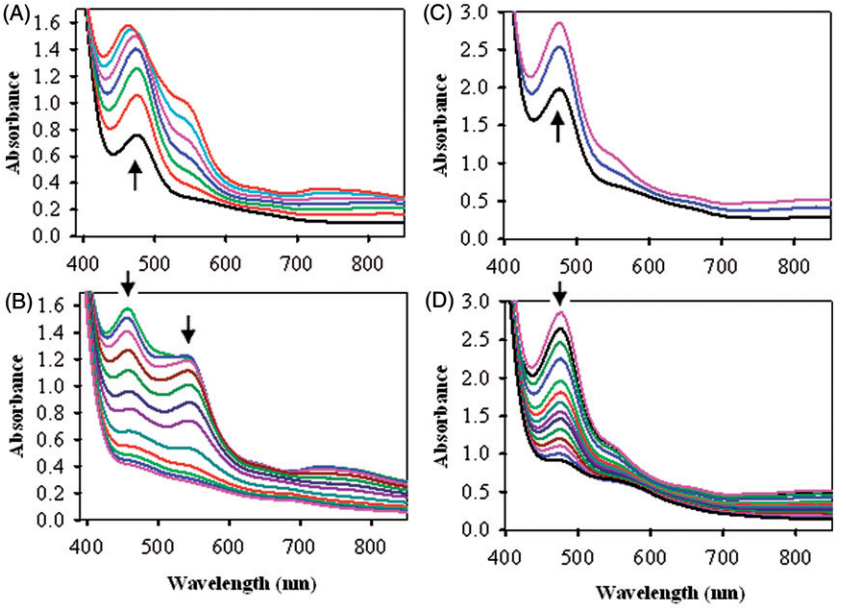

Figure 4. Panel A: Development of the 543 nm peak for formation of $Cr(O_2)^{2+}$ due to dioxygen binding to $[Cr(H_2O)(L^{ISQ})_2]$ (**1**) (7.2×10^{-4} mol L^{-1}) in DMF containing CH_3OH in the presence of air at RT. Spectra were recorded at 2-min intervals. Panel B: After reaching maximum intensity at 543 and 456 nm (top red curve shown in Panel A), absorbance of all bands started decreasing in intensity ultimately producing a weakly absorbing species in the visible region. Panel C: When **1** is dissolved in DMF (8.12×10^{-4} mol L^{-1}) in the presence of nitrogen at RT, the intensity of the 474 nm peak slowly increases but there is no development of the 543 nm peak (for formation of $Cr(O_2)^{2+}$) in the absence of air. Spectra were recorded at 2-min intervals. Panel D: After reaching maximum intensity at 474 nm (purple curve recorded at 6th min, shown in Panel C), absorbance started decreasing ultimately producing weakly absorbing species in the visible region.

the bands, and it continues to increase up to 10 min (purple curve) when a shoulder at 543 nm started growing and the band at 474 nm shifted to higher energy at 13th min (cyan curve). Ultimately the peaks are at 456 and 543 nm along with a weak broad band in the 700–850 nm region when they reached maximum intensity at 20 min [figure 4 (panel A, top red curve)].

Then the intensities of all these bands in the visible and NIR regions start decreasing with time, ultimately leading to very low absorbing species in the visible region [figure 4 (panel B)]. The whole process took 2 h for the entire change as compared to >3 h for the overall change when only DMF was used as solvent.

3.6.3. DMF solution in the presence of dry nitrogen. Very different electronic spectral results were obtained when **1** was dissolved in carefully degassed DMF with dry nitrogen and the spectral change was studied in the absence of air or oxygen. The spectral change of **1** in DMF in the presence of N_2 is shown in figure 4 (panels C and D). Initially it displayed a peak at 474 nm [figure 4 (panel C, black curve)] as observed in the very first scan in the presence of air [figure 3 (panel A), figure 4 (panel A)], and it started growing in intensity [figure 4 (panel C)] as observed in the presence of methanol [figure 4 (panel A)]. However, this peak at 474 nm reached

maximum intensity in 8 min [figure 4 (panel C, purple curve)] and then started decreasing slowly with time until it became steady within 3 h [figure 4 (panel D)]. There was no growth of a peak at 543 nm in the absence of air in contrast to that observed in the presence of air and methanol [figure 4 (panels A and B)] and no new peak developed at 548 nm as observed in the presence of air [figure 3 (panels A and B)].

Thus, it is clearly evident from figure 4 (panels A and C) that the increase in intensity of the band at 474 nm is neither due to dioxygen binding nor to any aerobic oxidation of the compound since this increase is also observed in nitrogen atmosphere [figure 4 (panel C)]. These observations strongly suggest that the increase in intensity of the band at 474 nm is likely associated with the immediate and spontaneous change in conductivity and pH of the DMF solution of **1** (figure S4). However, the increase in intensity of the peak at 543 nm along with the spectral shift of the 474 nm band [figure 4 (panels A and B)] in the presence of air and methanol is due to dioxygen binding to the species that is responsible for the 474 nm peak. The intensity of the peak at 543 nm gradually increases only when CH_3OH is already present in DMF before dissolving **1** in the presence of air. CH_3OH acts as a scavenger of CrO^{2+}, and thus helps in directly producing $Cr(O_2)^{2+}$ from the reaction of Cr^{2+} with dioxygen. This observation is very similar to that observed by Scott *et al.* [5, 6] in aqueous medium in the presence of CH_3OH leading to the formation of $[(H_2O)_5Cr(O_2)]^{2+}$ as indicated from the increased absorbance at 290 and 245 nm. The large red-shift in the band position in our case is not unlikely with the present ligand environment for the superoxo-Cr^{3+} species in this non-aqueous DMF medium, because it is known that for a CT band a shift of large magnitude is not unreasonable with a change in solvent [37] as well as in ligand environment. After reaching maximum intensity it starts decaying with time [figure 4 (panel B)]. When CH_3OH is not present, though $Cr(O_2)^{2+}$ is initially produced as evident from the shoulder at 543 nm in the very first scan of figure 3 (panel A, black curve), and reaching maximum intensity in about 6 min [red curve, second scan, figure 3 (panel A)], then it is rapidly converted to CrO^{2+} species as indicated from the spectral change shown in the 3rd and fourth scans [green and purple curves, respectively, figure 3 (panel A)]. This is consistent with the observation of Scott *et al.* [5, 6] that if addition of methanol was delayed by a few minutes in the reaction medium, there was no formation of $Cr(O_2)^{2+}$. The intense electronic absorptions appearing in the visible region due to CT transitions in different species formed in DMF solution of **1** in presence and/or absence of air along with their tentative assignments are presented in table 2.

Thus, based on the electronic spectral results of **1** in the absence and presence of methanol and air the sequence of events after its deprotonation shown in equation (1) can be explained by the following reactions:

$$\left[Cr(OH)(L^{ISQ})_2\right]^- + O_2 \rightarrow \left[Cr(O_2)(OH)(L^{ISQ})_2\right]^- \quad (2)$$

$$\left[Cr(O_2)(OH)(L^{ISQ})_2\right]^- + \left[Cr(OH)(L^{ISQ})_2\right]^- \rightarrow 2\left[O=Cr(OH)(L^{ISQ})_2\right]^- \quad (3)$$

$$\left[O=Cr(OH)(L^{ISQ})_2\right]^- + CH_3OH \rightarrow \left[Cr(OH)(L^{ISQ})_2\right]^- + HCHO + H_2O \quad (4)$$

$$\left[Cr(OH)(L^{ISQ})_2\right]^- + O_2 \rightarrow \left[Cr(O_2)(OH)(L^{ISQ})_2\right]^- \quad (5)$$

Table 2. Intense electronic spectral bands in the visible region due to CT transitions in different species formed in DMF solution of **1** in the presence and/or absence of air.

Band positions (nm)	Tentative assignments	Associated with the species formed in DMF solution
474	$L \rightarrow Cr(II)$ CT	$[Cr(OH)(L^{ISQ})_2]^-$
456	$L \rightarrow M$ CT	$[Cr(O_2)(OH)(L^{ISQ})_2]^-$
543	$M \rightarrow L$ (O_2) CT	
464	$L \rightarrow Cr(IV)$ CT	$[O{=}Cr(OH)(L^{ISQ})_2]^-$
548	oxo $\rightarrow Cr(IV)$ CT	
464	$L \rightarrow Cr(V)$ CT	$[O{=}Cr(OH)(L^{ISQ})_2]$

$$Cr^{IV}(OH) + Mn^{II} \rightarrow Cr^{IV}\text{–}OH\text{–}Mn^{II} \rightarrow Cr^{III}\text{–}OH + Mn^{III}$$

$$Cr^{IV}(OH) + Mn^{III} \rightarrow Cr^{IV}\text{–}OH\text{–}Mn^{III} \rightarrow Cr^{V}\text{–}OH + Mn^{II}$$

Scheme 4. Proposed mechanism for the Mn^{2+} catalyzed disproportionation reaction.

In the absence of methanol, the formation of the CrO^{2+} intermediate shown in equation (3) is rapid and its concentration becomes maximum within 14 min when the 548 nm peak reaches maximum intensity [figure 3 (panel A)]. The 548 nm peak originates from this CrO^{2+} intermediate is due to the following observations: (1) when methanol is already present along with DMF, this peak is not observed. Instead, a peak around 543 nm is seen. (2) The intensity of the 548 nm peak rapidly decays when methanol or Mn^{2+}, scavengers of CrO^{2+}, is added when 548 nm peak reaches maximum intensity. (3) In the presence of PPh_3 the 548 nm peak could not develop (*vide infra*), and (4) It can damage DNA only when this peak reaches maximum intensity.

The disappearance of CrO^{2+} may be involved in the following reaction as suggested by different researchers [6, 38, 39]:

$$CrO^{2+} + Cr^{2+} + H_2O \rightarrow \left[Cr(OH)_2Cr\right]^{4+} \quad (6)$$

or it may undergo disproportionation as suggested by Gould and Ghosh *et al.* [18, 19] for their reported Cr(IV) complex $[Cr^{IV}O(EHBA)_2]$, where EHBA = 2-ethyl-2-hydroxybutanoate anion, who have shown that the deprotonated $Cr^{IV}(OH)$ generated in solution undergoes disproportionation to produce almost equivalent quantities of Cr(III) and Cr(V). The same $Cr^{IV}(OH)$ species was involved in Mn^{2+} catalyzed disproportionation, and its mechanism has been proposed by Gould and coworkers [18, 19] as shown in scheme 4.

We suggest a similar mechanism is also operating for Mn^{2+} catalyzed disproportionation shown in figure 3 (panel C) for **1** in DMF and the two-exponent fit of this kinetic data indicates involvement of two species associated with the decay of the 548 nm peak in the presence of Mn^{2+} ion and is consistent with the proposed mechanism shown in scheme 4. The principal route that utilizes the activated complex $Cr^{IV}\text{–}OH\text{–}Mn^{II}$ in the presence of excess Mn(II) and the minor route involving the Mn(III) species account for the large difference in k_1 and k_2 observed for **1**. Thus this latter proposition for disproportionation is more logical in this non-aqueous medium and we strongly believe

that deprotonation of the aqua ligand and increase in conductivity followed by decrease in pH of the DMF solution is associated with formation of a $Cr^{II}(OH)$ species which binds to O_2 to form the superoxo-Cr(III) compound shown in equation (2) and its rapid and subsequent conversion to $[O{=}Cr(OH)(L^{ISQ})_2]^-$ as shown in equation (3). In the absence of Mn^{2+}, this $[O{=}Cr(OH)(L^{ISQ})_2]^-$ species undergoes uncatalyzed disproportionation, as suggested by Gould [18] and Ghosh *et al.* [19] for their Cr(IV) complex $[Cr^{IV}O(EHBA)_2]$ mentioned earlier, leading to formation of a Cr^V and a $Cr^{III}(OH)$ complex. This is supported by the observation of the EPR signal of a d^1 Cr^V species from the DMF solution of **1** at RT already discussed and a stable Cr(III) compound, $[Cr(OH)(DMF)(L^{ISQ})_2]$ (**2**), has also been isolated and characterized from this DMF solution after completion of the disproportionation.

The hypothesis for formation of an ionic $Cr^{IV}(OH)$ species in the presence of air is also supported by the following observations. When **1** is dissolved in DMF that already contains $[N(n\text{-}Bu)_4]PF_6$, which is used as a supporting electrolyte, the 474 and 543 nm peaks are not seen even in the first scan (within the same span of time used for all other cases). The very first scan within 2 min [figure 5 (panel A, black curve with dotted line)] resulted in peaks at 548 and 455 nm directly and these two peaks reached maximum intensity within 4 min [figure 5 (panel A, top red curve)]. Then their intensity started decreasing as revealed in the third scan (6th min, green curve). This clearly suggests that deprotonation of the initial complex followed by dioxygen binding to the deprotonated species and the conversion of the $Cr(O_2)^{2+}$ to CrO^{2+} in the presence of $[N(n\text{-}Bu)_4]PF_6$ becomes much faster compared to that in its absence (the peak at 548 nm reaches maximum intensity in 14 min in the absence of $[N(n\text{-}Bu)_4]PF_6$) and also the decay of the 548 nm peak is completed within 80 min in the presence of $[N(n\text{-}Bu)_4]PF_6$ [figure 5 (panel B)] as compared to >3 h required in its absence [figure 3 (panel B)]. Thus, both the rate of formation and the rate of decay of CrO^{2+} are enhanced in the presence of $[N(n\text{-}Bu)_4]PF_6$, indicating that both these steps are associated with ionic species whose formations are favored in the presence of a supporting electrolyte. Since the uncatalyzed disproportionation [18, 19] of $[O{=}Cr(OH)(L^{ISQ})_2]^-$ is slow in the absence of $[N(n\text{-}Bu)_4]PF_6$, it is expected that the concentration of the d^1 Cr(V) complex should increase slowly with time, consistent with observation of initial increase in Cr(V) EPR signal intensity (figure S3) of the DMF solution of **1** at RT. Also, the appearance of the d^1 Cr(V) EPR signal at RT indicates that the unpaired spins of the two L^{ISQ} ligands in $[O{=}Cr(OH)(L^{ISQ})_2]$ are also strongly antiferromagnetically coupled [12, 14] resulting in a $S_t = ½$ system.

Our contention that the rate of formation as well as decay (of the CrO^{2+} species) is enhanced in the presence of other ions is further supported from the results obtained in the presence of KSCN. The very first scan within 2 min exhibited a strong peak at 474 nm along with a broad shoulder at 543 nm, but the second scan within 5 min yielded two strong peaks at 453 and 543 nm reaching maximum intensity and then started decaying even faster than in the presence of $[N(n\text{-}Bu)_4]PF_6$ and completed within 80 min (figure S8), but the band at 548 nm shifts to 543 nm indicating the coordination of NCS^- to metal, possibly forming $[O{=}Cr(NCS)(L^{ISQ})_2]^-$. Thus, the presence of a stronger anionic ligand leads to faster disproportionation of the O=Cr(IV) complex possibly by enhancing the internal electron transfer associated with the activated complex formed, as proposed by Gould and coworkers [18, 19] during disproportionation to form the uncharged O=Cr(V) species, $[O{=}Cr(NCS)(L^{ISQ})_2]$ in our case along with a Cr(III) complex. Since no IVCT band [22, 23] was observed in the electronic

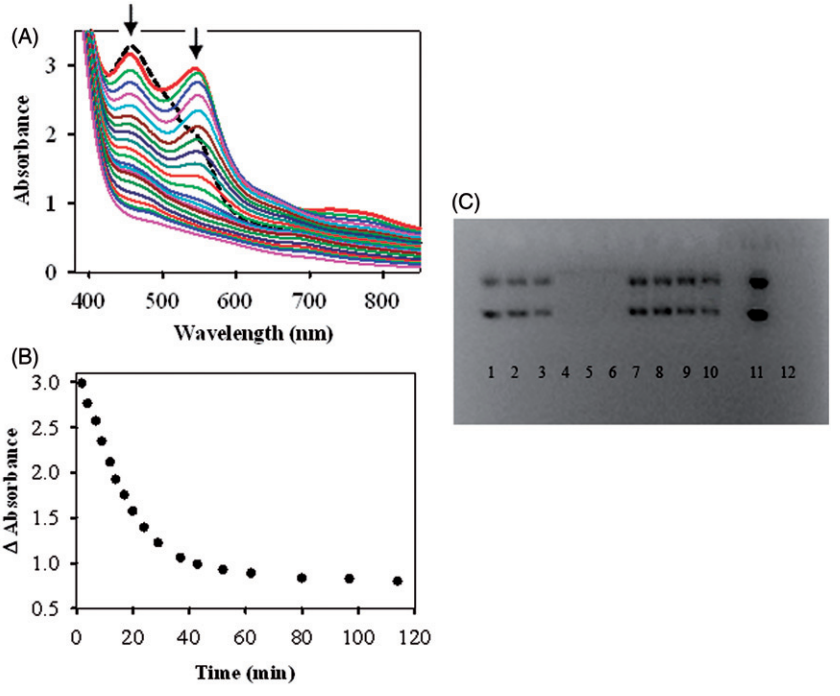

Figure 5. Panel A: Electronic spectral change of $[Cr(H_2O)(L^{ISQ})_2]$ (**1**) (0.87×10^{-3} mol L^{-1}) in DMF containing excess $[N(n\text{-}Bu)_4]PF_6$ in the presence of air: Black dotted curve is the very first scan within 1 min. Top red curve is the second scan within 4 min. Then the intensities of all bands in this region start decreasing with time leading to low absorbing products in this region. Panel B: Plot of absorbance change for the disappearance of the band at 548 nm *vs.* time for $[Cr(H_2O)(L^{ISQ})_2]$ (**1**) in DMF containing excess $[N(n\text{-}Bu)_4]PF_6$. Panel C: DNA interaction results. Lane 1: 5th min, lane 2: 11th min; lane 3: 12th min; lanes 4, 5, 6, 7, 8, 9, and 10 are for 13th, 14th, 15th, 16th, 17th, 18th, and 19th min, respectively. Lane 11: negative control (DNA in TAE); lane 12: positive control (DNA treated with DNaseI for 30 min at room temperature).

spectrum of any reaction products after completion of decomposition reactions mentioned so far, and since these reactions were carried out in presence of air, it is likely that the decomposition products Cr(III) and Cr(V) also contain the oxidized *o*-iminothionebenzosemiquinonate(1−) π-radical $(L^{ISQ})^{1-}$.

Lastly, we studied the electronic spectral change of **1** in DMF in the presence of two-fold excess of PPh_3 which is known [5, 10] to readily react with O=Cr(IV) to produce $O{=}PPh_3$ and a Cr(II) species. The spectral change is shown in figure S9. The very first scan within 2 min, as expected, displayed a strong peak at 474 nm with a shoulder around 543 nm (black dotted curve *a*, figure S9) in the presence of PPh_3. However, the growth of the peak at 543 nm is severely affected as evident in the second scan (red curve *b*) within 5 min and found to decrease further in the third scan (green curve *c*) within 8 min. This clearly indicates that the species associated with this peak disappears faster in the presence of PPh_3. The overall absorbance at completion of the reaction (<35 min) is found to be much lower [figure S9 (panels A, B)] as compared to all other cases. This could be due to formation of low absorbing Cr(II) compound in the present case. It appears in the present case that the O=Cr(IV) complex produced from the superoxo-Cr(III) species (generated after dissolving **1** in DMF in the presence of air)

reacts faster [5] with PPh_3 and hence the possibility of its disproportionation is drastically minimized thereby reducing the concentration of the O=Cr(V) species formed; if formed, it will also react with PPh_3, thereby producing only Cr(II) and Cr(III) species which are expected to be low absorbing in this region. Evaporation of this solution after completion of reaction with PPh_3 followed by purification yielded $O{=}PPh_3$ and a mixture of unknown chromium compounds. Thus, the absence of the 548 nm peak and the formation of $O{=}PPh_3$ strongly suggest that the generated O=Cr(IV) reacts immediately with PPh_3 causing oxo transfer. It was observed that exposure of the final solution to air after the completion of the reaction with either methanol or PPh_3 did not cause any spectral change or color change of the solution, indicating that the final Cr-product does not react with air/oxygen, possibly due to the formation of μ−oxo Cr(III) dimer [10, 40].

3.7. *DNA interaction*

As mentioned in the experimental section, samples drawn up to the 12th min from the time of making the DMF solution of **1** were unable to damage DNA. This is represented by the samples taken at the 5th, 11th, and 12th min, each reacting separately with the DNA solutions for 30 s, and then added with the DNA loading dye and placed in individual wells of the gel [lanes 1–3, figure 5 (panel C)], which clearly show that the DNA remains unaffected. However, when the samples taken at the 13th, 14th, and 15th min reacted with DNA solutions for 30 s, and the mixtures were then added with DNA loading dye and placed in the individual wells of the gel (lanes 4–6), the DNA is completely wiped out as revealed from these lanes [lanes 4–6, figure 5 (panel C)]. The samples drawn during 16th–19th min, however, show no effect on the DNA (lanes 7–10). There are many species generated in the DMF solution of **1** and the concentrations of these species change with time as revealed from both electronic and EPR spectral studies discussed earlier. However, the species generated and/or present within the period of 13th–15th min from the time of making the DMF solution of **1** are responsible for damaging DNA. The fact that the absorbance of the 548 nm peak associated with the highly reactive Cr^{IV} species, as determined from reactions of this compound with PPh_3, methanol and Mn^{2+} ion, attains maximum intensity in the 14th min, is significant as it coincides with the timing (13th–15th min from the time of making the DMF solution of **1**) of the generated species that is capable of DNA damage. Thus DNA damage is observed only when the concentration of Cr^{IV} species is maximum. These results strongly suggest that the highly reactive O=Cr(IV) intermediate, $[O{=}Cr(OH)(L^{ISQ})_2]^-$, is mainly responsible for the DNA damage, and not the Cr(V) species since the activity for DNA damage is observed only up to the 15th min from the time of making the DMF solution of **1**, though the Cr(V) concentration in solution remains large even after that period as evident from its EPR signal intensity. Sugden and Wetterhahn [36] have shown in their work of Cr(V)−mediated nucleotide oxidation in reactions of bis(2-ethyl-2-hydroxybutyrato)oxochromate(V) $[CrO(EHBA)_2]^-$ with thymidine nucleotides that the production of thiobarbituric acid reactive species and thymine release correlated with decay of the Cr(V) EPR signal. Also, they have suggested that only Cr(IV) formed upon disproportionation of Cr(V) [41], oxidized the nucleotide deoxyribose sugar moiety *via* a phosphate-bound intermediate and not Cr(V). Very recently, Saha *et al*. have reviewed the sources and

toxicity of hexavalent chromium [42] where they have pointed out that reduction of hexavalent chromium by cellular reductants to Cr(V), Cr(IV), and Cr(III) has been considered an important step toward chromium induced carcinogenicity [43, 44]. During reduction of Cr(VI) to Cr(III) *via* Cr(V) and Cr(IV) intermediates, interaction with DNA is responsible for carcinogenesis [42–44]. It has also been found in certain cases that free radicals generated by Cr(V) and Cr(IV) intermediates cause DNA strand breaks and are suggested to be important in the mechanism of chromium induced carcinogenicity [45]. This latter possibility that these Cr(IV) and Cr(V) species generate free radicals that may also cause DNA strand breaks [42, 45] is less likely in our case under the experimental conditions. We strongly believe that the highly reactive O=Cr(IV) species that reaches maximum concentration in the 14th min from the time of making the DMF solution of **1** in the presence of air is mainly responsible for interacting with DNA and its complete cleavage because this cleavage is observed only in the 13th–15th min time period when the concentration of this O=Cr(IV) species is maximum.

3.8. *Electrochemical results*

The redox behavior of **1** has been studied in DMF containing 0.1 M TEAP at a platinum working electrode using cyclic voltammetry under nitrogen; this whole experiment was completed within 5 min. For an initial negative scan between 0 and −1.50 V, there is a reduction peak near −1.14 V, reversal of the scan gives two weak anodic peaks at −0.94 and −0.35 V, respectively, and these are coupled to the reduction wave at −1.14 V, evident from multiple scans in this potential range [figure 6(a)]. The initial cathodic wave at −1.14 V [figure 6(a)] is most likely due to reduction, as shown in equation (7), of the deprotonated species $[Cr(OH)(L^{ISQ})_2]^-$ that is generated immediately after making the DMF solution and found to be stable up to 8 min in nitrogen as revealed from the electronic spectral study shown in figure 4 (panel C).

$$\left[Cr(OH)(L^{ISQ})_2\right]^- + e^- \rightarrow \left[Cr(OH)(L^{ISQ})_2\right]^{2-} \quad (7)$$

For an initial positive scan between 0 and +1.80 V, two irreversible oxidation waves are observed at +0.48 and +0.92 V, respectively [figure 6(b)]. The first oxidation wave at +0.48 V is due to

$$\left[Cr(OH)(L^{ISQ})_2\right]^- \rightarrow \left[Cr(OH)(L^{ISQ})_2\right] + e^- \quad (8)$$

and this oxidized species $[Cr(OH)(L^{ISQ})_2]$ undergoes further oxidation at +0.92 V.

When the potential is scanned from −1.50 to +1.80 V starting with an initial negative scan, all the above-mentioned cathodic and anodic peaks are observed. However, a second cycle starts yielding two new reductive responses at −0.02 and −0.52 V, which become prominent in the third cycle [figure 6(c)]. These two new cathodic responses at −0.02 and −0.52 V are associated with the species which are irreversibly oxidized at +0.48 and +0.92 V, because these two peaks are not observed if the potential is scanned only between 0 to +2 V or 0 to −2 V, respectively, [figure 6(a, b)]. This strongly suggests that the oxidized species at +0.92 V undergoes two successive reductions at −0.02 and −0.52 V, respectively, producing the initial species, $[Cr(OH)(L^{ISQ})_2]^-$, because this is

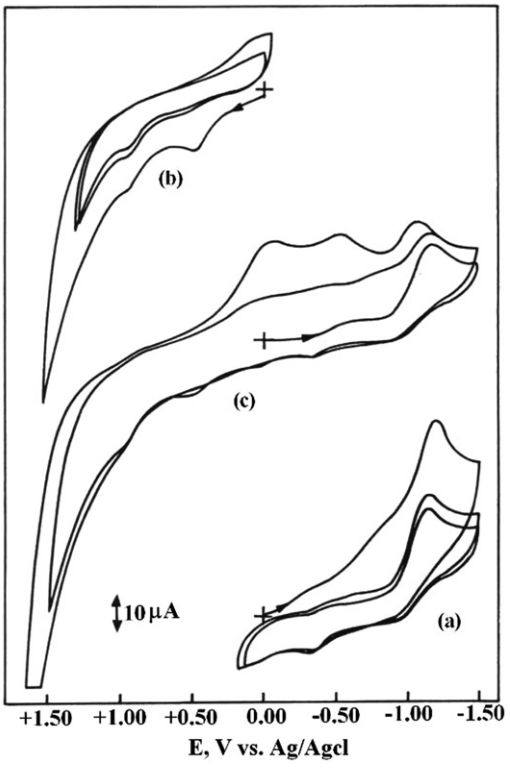

Figure 6. Cyclic voltammograms for **1** (2.5×10^{-3} mol L^{-1}) in DMF containing 0.1 M TEAP (a) at a scan rate of 400 mVs^{-1}, (b) at a scan rate of 600 mVs^{-1}, and (c) at a scan rate of 200 mVs^{-1}, respectively.

found to be reduced again at the same potential −1.14 V (observed in initial negative scan between 0 and −1.50 V) as revealed from the multiple scans shown in figure 6(c).

It is very clear from the cyclic voltammogram of **1** that its electrochemical behavior is complex and moreover, it is very different from that reported by Wieghardt and coworkers [22] for tris(dioxolene)chromium and tris(dithiolene)chromium complexes of the electron-transfer series $[Cr(dioxolene)_3]^z$ and $[Cr(dithiolene)_3]^z$, and **1** does not belong to any such electron-transfer series.

4. Conclusions

The Cr(II) compound $[Cr(H_2O)(L^{ISQ})_2]$ (**1**) containing the *o*-iminothionebenzosemiquinonate(1−) ligand π-radical is highly stable in the solid state in the presence of air but undergoes spontaneous aerobic oxidation in DMF to produce a superoxo−Cr(III) species which in turn produces another highly reactive intermediate O=Cr(IV) that decays with time resulting in an oxo−Cr(V) compound and a Cr(III) compound. Electronic and EPR spectral studies of DMF solutions of **1** at RT indicate that a number of species are generated; we did not attempt to separate and isolate them

from solutions except one Cr(III) end product, $[Cr(OH)(DMF)(L^{ISQ})_2]$ (**2**). Several attempts to grow crystals for **2** were unsuccessful, so it has not been possible to determine its crystal structure. However, isolation of $O{=}PPh_3$ from reaction media strongly suggests formation of O=Cr(IV) and/or O=Cr(V) species during decomposition of **1** in the presence of air. Thus, it is shown that aerial oxidation of lower oxidation state in non-aqueous medium produces reactive intermediates Cr(IV) and Cr(V) which are normally observed during reduction of Cr(VI) to Cr(III) in aqueous medium, and may lead to very high toxicity.

Supplementary material

Figure S1: IR spectrum of **1**. Figure S2: XPS spectrum of **1** showing N 1s and O 1s peaks. Figure S3: EPR spectral change of **1** in DMF solution at RT showing the initial increase in signal intensity with time. Figure S4: Plot of pH change *versus* time of a fresh DMF solution of 4.43×10^{-4} M $[Cr(H_2O)(L^{ISQ})_2]$ (**1**) at RT in the presence of air. Figure S5: Decay of the 548 nm peak in presence of PPh_3 after it reached maximum intensity. Figure S6: Reaction with PPh_3 when the 548 nm peak almost disappeared. Figure S7: Decay of 548 nm peak after addition of 1.0 mM CH_3OH when reached maximum intensity. Figure S8: Plot of absorbance change at 543 nm *versus* time for **1** in DMF containing two-fold excess KSCN in the presence of air. Figure S9: Electronic spectral change of **1** in DMF containing two-fold excess PPh_3 in the presence of air.

Acknowledgments

M.K. thanks the Department of Inorganic Chemistry, Indian Association for the Cultivation of Science, Kolkata, for the help with the elemental analysis and IR spectrum. We thank the SAIF, IIT-Madras for EPR and magnetic moment measurements and CLRI for providing EPR facilities. A.P.K. thanks Dr C.S. Gopinath, Catalysis Division, National Chemical Laboratory, Pune, for his help with the ESCA studies. P.T.M. thanks the DST, Govt. of India for Ramanna Fellowship (SR/S1/RFIC-02/2006) and also the INSA for its Senior Scientistship. We thank the Reviewers for their valuable suggestions to improve the manuscript.

References

[1] M.R. Bukowski, K.D. Koehntop, A. Stubna, E.L. Bominaar, J.A. Halfen, E. Münck, W. Nam, L. Que Jr. *Science*, **310**, 1000 (2005), and references therein.
[2] J.-U. Rohde, J.-H. In, M.H. Lim, W.W. Brennessel, M.R. Bukowski, A. Stubna, E. Münck, W. Nam, L. Que Jr. *Science*, **299**, 1037 (2003).
[3] M.H. Lim, J.-U. Rohde, A. Stubna, M.R. Bukowski, M. Costas, R.Y.N. Ho, E. Münck, W. Nam, L. Que Jr. *Proc. Natl. Acad. Sci. U.S.A.*, **100**, 3665 (2003).
[4] A. Decker, J.-U. Rohde, L. Que Jr, E.I. Solomon. *J. Am. Chem. Soc.*, **126**, 5378 (2004).
[5] S.I. Scott, A. Bakac, J.H. Espenson. *J. Am. Chem. Soc.*, **113**, 7787 (1991).
[6] S.I. Scott, A. Bakac, J.H. Espenson. *J. Am. Chem. Soc.*, **114**, 4205 (1992).

[7] (a) A. Hess, M.R. Horz, L.M. Liable-Sands, D.C. Linder, A.L. Rheingold, K.H. Theopold. *Angew. Chem. Int. Ed.*, **38**, 166 (1999); (b) K. Qin, C.D. Incarvito, A.L. Rheingold, K.H. Theopold. *Angew. Chem. Int. Ed.*, **41**, 2333 (2002).
[8] (a) J. Cho, J. Woo, W. Nam. *J. Am. Chem. Soc.*, **132**, 5958 (2010); (b) J. Cho, J. Woo, J.E. Han, M. Kubo, T. Ogura, W. Nam. *Chem. Sci.*, **2**, 2057 (2011).
[9] J.R. Budge, B.M.K. Gatehouse, M.C. Nesbit, B.O. West. *J. Chem. Soc., Chem. Commun.*, 370 (1981).
[10] J.T. Groves, W.J. Kruper Jr, R.C. Haushalter, W.M. Butler. *Inorg. Chem.*, **21**, 1363 (1982).
[11] K.H. Nill, F. Wasgestian, A. Pfeil. *Inorg. Chem.*, **18**, 564 (1979).
[12] D. Herebian, E. Bothe, E. Bill, T. Weyhermuller, K. Wieghardt. *J. Am. Chem. Soc.*, **123**, 10 012 (2001).
[13] H. Chun, T. Weyhermuller, E. Bill, K. Wieghardt. *Angew. Chem. Int. Ed.*, **40**, 2489 (2001).
[14] P. Ghosh, E. Bill, T. Weyhermuller, K. Wieghardt. *J. Am. Chem. Soc.*, **125**, 3967 (2003).
[15] L.F. Larkworthy, J.M. Murphy, D.J. Phillips. *Inorg. Chem.*, **7**, 1436 (1968).
[16] S.B. Waghmode, R. Vetrivel, S.G. Hegde, C.S. Gopinath, S.J. Sivasanker. *Phys. Chem. B*, **107**, 8517 (2003).
[17] M. Vijayaraj, C.S. Gopinath. *J. Catal.*, **241**, 83 (2006).
[18] E.S. Gould. *Coord. Chem. Rev.*, **135/136**, 651 (1994), and references therein.
[19] M.C. Ghosh, E. Gelerinter, E.S. Gould. *Inorg. Chem.*, **31**, 702 (1992).
[20] K. Nakamoto. *Infrared and Raman Spectra of Inorganic and Coordination Compounds, Part B, Applications in Coordination, Organometallic, and Bioinorganic Chemistry*, 5th Edn, p. 54, Wiley, New York (1997).
[21] A.P. Koley, R. Nirmala, L.S. Prasad, S. Ghosh, P.T. Manoharan. *Inorg. Chem.*, **31**, 1764 (1992).
[22] R.R. Kapre, E. Bothe, T. Weyhermuller, S. DeBeer George, N. Muresan, K. Wieghardt. *Inorg. Chem.*, **46**, 7827 (2007).
[23] R.R. Kapre, E. Bothe, T. Weyhermuller, S. DeBeer George, K. Wieghardt. *Inorg. Chem.*, **46**, 5642 (2007).
[24] T. Petrenko, K. Ray, K.E. Wieghardt, F. Neese. *J. Am. Chem. Soc.*, **128**, 4422 (2006).
[25] K. Ray, T. Weyhermüller, F. Neese, K. Wieghardt. *Inorg. Chem.*, **44**, 5345 (2005).
[26] K. Ray, A. Begum, T. Weyhermüller, S. Piligkos, F. Neese, K. Wieghardt. *J. Am. Chem. Soc.*, **127**, 4403 (2005).
[27] K. Ray, E. Bill, T. Weyhermüller, K. Wieghardt. *J. Am. Chem. Soc.*, **127**, 5641 (2005).
[28] K. Ray, T. Weyhermüller, A. Goosens, M.W. Crajé, K. Wieghardt. *Inorg. Chem.*, **42**, 4082 (2003).
[29] C.D. Wagner, W.M. Riggs, L.E. Davis, J.F. Moulder, G.F. Muilenberg. *Handbook of X-ray Photoelectron Spectroscopy*, Perkin–Elmer Corporation, Physical Electronics Division, Eden Prairie, MN (1979).
[30] M. Cardona, L. Ley. *Photoemission from Solids*, Springer Verlag, Heidelberg (1978).
[31] M. Cardona, L. Ley (Eds.), *Photoemission in Solids I: General Principles*, Springer-Verlag, Berlin (with additional corrections) (1978).
[32] J.C. Fuggle, N. Mårtensson. *J. Electron Spectrosc. Relat. Phenom.*, **21**, 275 (1980).
[33] D.T. Clark, D.B. Adams. *Chem. Phys. Lett.*, **10**, 121 (1971).
[34] T.L. Siddall, N. Miyaura, J.C. Huffman, J.K. Kochi. *J. Chem. Soc., Chem. Commun.*, 1185 (1983).
[35] A. Bakac. *J. Am. Chem. Soc.*, **122**, 1092 (2000).
[36] K.D. Sugden, K.E. Wetterhahn. *J. Am. Chem. Soc.*, **118**, 10 811 (1996).
[37] O. Pestovsky, A. Bakac. *Dalton Trans.*, 556 (2005).
[38] M. Ardon, R.A. Plane. *J. Am. Chem. Soc.*, **81**, 3197 (1959).
[39] R.W. Kolaczkowski, R.A. Plane. *Inorg. Chem.*, **3**, 322 (1964).
[40] J.K. Kochi, J.W. Powers. *J. Am. Chem. Soc.*, **92**, 137 (1970).
[41] M. Krumpolc, J. Rocek. *Inorg. Chem.*, **24**, 617 (1985).
[42] R. Saha, R. Nandi, B. Saha. *J. Coord. Chem.*, **64**, 1782 (2011), and references therein.
[43] (a) J.K. Wetterhahn. *J. Am. Chem. Soc.*, **104**, 874 (1982); (b) G.R. Borthiry, W.E. Antholine, J.M. Myers, C.R. Myers. *J. Inorg. Biochem.*, **102**, 1449 (2008).
[44] (a) A.M. Standeven, K.E. Wetterhahn. *Pharmacol. Toxicol.*, **68**, 469 (1991); (b) L. Cheng, D.M. Sonntag, J. de Boer, K. Dixon. *J. Environ. Pathol. Toxicol. Oncol.*, **19**, 239 (2000).
[45] J.A. Schmidt, A.W. Andren. In *Nickel in the Environment*, J.O. Nriagu (Ed.), pp. 93–136, Chap. 6, John Wiley and Sons, New York (1980).